Predictive Stator Current Control of a Five-phase Motor using a Hybrid Control Set

Manuel R. Arahal, Federico Barrero, Mario Bermúdez, and Manuel G. Satué

***Abstract*—Finite state model predictive control of multi-phase drives can use an extra number of inverter configurations compared to the three-phase case. This, however, requires more computing power for the optimization phase. The application time of each selected voltage vector is then increased, which can result in higher harmonic content. Reducing the allowed voltage vectors can speed up the computations, thus ameliorating the current tracking/regulation in the different orthogonal subspaces. However, the flexibility offered by the reduced set of voltage vectors is less than that of the full set. Furthermore, a lower sampling time can result in an increase of the switching frequency, especially for some speed-load combinations. This paper proposes the use of a hybrid scheme where the set of allowed voltage vectors is not fixed but rather selected on-line according to the actual speed and torque producing stator current which are computed by the outer loop. A five-phase induction machine is used as a test bed for the proposal, showing improved results with respect to the nonhybrid case.**

***Index Terms*—Induction Machines, Multi-phase systems, Performance map, Predictive control, Voltage vectors.**

I. Introduction

MODEL Predictive Control (MPC) has recently been explored as a versatile control technique for systems using power converters [1], [2]. Control strategies for tracking of current, torque, and speed have been successfully implemented [3], [4]. In the realm of multi-phase drives, Finite State MPC (FSMPC) applied for the tracking of stator currents is arguably one of the most popular techniques [5]. It easily allows to treat the extra number of phases and, at the same time, consider different electro-mechanical issues relevant to control applications [6], [7]. It is well known that FSMPC needs a fair amount of computing time for the optimization of the Cost Function (CF). The sampling time is then limited by the computing time, and this means that the application time of the selected Voltage Vector (VV) is also increased [8].

The use of Virtual Voltage Vectors (VVV) [9], [10] in multi-phase drives has been proposed to cope with this issue for different number of phases and for different types of machines [11]–[13], where the number of utilized VVV is notably restrained to avoid an increment of the controller computing time, in opposition to conventional three-phase systems [14], [15]. The basic VVV scheme combines two VV within one sampling period in a way that zero average amplitudes are produced in the $x-y$ subspace. However, the $x-y$ current is not really under control since there is not a closed loop to regulate it [16]. To alleviate these problems, combinations of VVV have been proposed in [17]. In addition, other works have proposed alternative schemes. For instance, in [18] an adaptive control set method based on VV with different amplitudes is used. In [19] a feed-back mechanism is used to achieve with short horizon cost functions similar results as those obtained with long horizons [20], but without the computational burden. As a result, a convenient trade-off between harmonic content and switching frequency is achieved. In [21], a flexible duty ratio optimization is used, considering all possible two-vector combinations and part of three-vector combinations.

Reducing the set of Allowable Voltage Vectors (AVV), results in a reduction of sampling time that can improve the harmonic content. For instance, using just the VV in the outermost circle plus a zero VV reduces the number of AVV of a five-phase inverter from 32 to 11 [22]. Non-uniform sampling time has also been proposed in this regard, by selecting the VV and its application time independently [8] or using a variable sampling frequency to reduce the average switching frequency to a low and quasi-constant level [23].

This paper presents a novel control scheme in which VV are selected from a Hybrid Control Set (HCS). The HCS includes several standard sets such as large VV, medium VV, and so on. In the proposal, for each combination of speed and i_q current, the most adequate set of AVV is selected on-line. This idea is supported by the concept of control methods such as Gain Scheduling [24]. These methods share the idea of dividing a nonlinear design problem into smaller sub-problems that might be treated more easily. Many variations can be found in the literature, including the strategy known as Local Controller Networks [25], where a set of controllers is considered instead of just a fixed one. At any given moment, just one controller from the set is allowed to actuate the system. The decision of which controller should be used is based on a handful of variables related to the current state of the system [26]. This scheme can work provided that, for each state, an adequate/optimal controller can be univocally determined. In this proposal, the controller is not modified, however, the set of allowable control actions is changed from one operation point to another.

Next section presents the FSMPC scheme for the case study, a five-phase Induction Machine (IM), and introduces the experimental setup used for the assessment and comparisons. The hybrid control structure or HCSMPC is then defined in Section III. Simulations and experimental assessment are

Manuscript received Xxx xx, 20xx; revised Xxx xx, 20xx. (*Corresponding author: Federico Barrero*).

M.R. Arahal and M.G. Satué are with Systems Engineering and Automation Department, University of Seville, Seville 41092 Spain (e-mail: arahal@us.es; mgarrido16@us.es).

F. Barrero is with the Electronic Engineering Department, University of Seville, Seville 41092 Spain (e-mail: fbarrero@us.es).

M. Bermúdez is with the Electrical Engineering Department, University of Seville, Seville 41092 Spain (e-mail: mbermudez4@us.es).

provided in Section IV, and the conclusions are drawn in the last section.

II. FSMPC OF A FIVE-PHASE MOTOR

Predictive control has found a wide variety of applications in the control of multi-phase drives, where the implementation requires a high computational cost due to the optimization phase. MPC techniques require a good knowledge of the parameters of the IM model and the particular case of FSMPC is best adapted to Voltage Source Inverter (VSI) control due to the limited number of switching states available in the power converter. Most of the research works in the field are related to the current regulation, and the outer loop is usually responsible for torque/speed regulation using a Proportional Integral (PI) controller. Its basis is the field-oriented control of the IM, where the flux and the electrical torque are independently controlled using reference currents i_{sd}^* to regulate the flux and i_{sq}^* to control the electrical torque.

In FSMPC control of multi-phase drives, the reference currents in $d-q$ plane are translated to the $\alpha-\beta$ space using the Park transformation, given by matrix D and the flux position θ_a, as follows

$$D = \begin{pmatrix} \cos\ \theta_a & \sin\ \theta_a \\ -\sin\ \theta_a & \cos\ \theta_a \end{pmatrix} \tag{1}$$

The objective of the FSMPC is to track the reference stator currents i_s^* in the $\alpha-\beta$ space, obtained from the reference currents in the $d-q$ plane, i_{sd}^* and i_{sq}^*. The reference stator currents i_s^* in the $x-y$ plane are set to zero in the present case, where a distributed winding machine is used. For this purpose, a discrete model of the physical system is used to predict the future behavior of the output variables $\hat{i}_s$ for each possible control vector u_j (the VSI gating signal). The prediction is computed using measured values of the mechanical speed ω_m (that is used to estimate rotor speed ω_r), and stator phase currents i_s. The most adequate control action u_{opt} is selected minimizing a cost function J. This control action is applied to the VSI during the next sampling period.

A symmetrical five-phase IM with distributed windings equally displaced $\vartheta = 2\pi/5$ and fed by a five-phase two-level VSI is considered. The drive modeling process is made using some standard assumptions: uniform air gap, symmetrical distributed windings, sinusoidal magneto-motive force (MMF) distribution, and negligible core and magnetic losses. The sinusoidal MMF distribution is a well-known assumption in conventional and multi-phase induction machines' modeling, provided that a distributed winding induction machine is used. Vector space decomposition is applied to produce a set of equations modelling the evolution of currents in the $\alpha-\beta$ sub-space (involved in fundamental flux and torque production), and $x-y$ sub-space (related to losses due to harmonics of the order $10n \pm 3$). Additionally, a zero sequence harmonic component of the order $5n$ with $n = 1, 2, 3, ...$ is projected in the z-axis, but it is not considered because the neutral point is isolated. Using $\alpha-\beta$ and $x-y$ stator currents and $\alpha-\beta$ rotor currents as state variables $x = (i_{s\alpha},\ i_{s\beta},\ i_{sx},\ i_{sy},\ i_{r\alpha},\ i_{r\beta})^T$, the following equations are found.

$$\dot{x}(t) = A(\omega_r(t))x(t) + Bv(t) \tag{2}$$
$$y(t) = Cx(t) \tag{3}$$

where $v = (v_{s\alpha},\ v_{s\beta},\ v_{sx},\ v_{sy})^T$ are the applied stator voltages and the output signals are the stator currents $y = (i_{s\alpha},\ i_{s\beta},\ i_{sx},\ i_{sy})^T$. Matrices A and B depend on the rotor electric speed ω_r.

$$A = \begin{pmatrix} -a_{s2} & a_{m4} & 0 & 0 & a_{r4} & a_{l4} \\ -a_{m4} & -a_{s2} & 0 & 0 & -a_{l4} & a_{r4} \\ 0 & 0 & -a_{s3} & 0 & 0 & 0 \\ 0 & 0 & 0 & -a_{s3} & 0 & 0 \\ a_{s4} & -a_{m5} & 0 & 0 & -a_{r5} & -a_{l5} \\ a_{m5} & a_{s4} & 0 & 0 & a_{l5} & -a_{r5} \end{pmatrix} \tag{4}$$

$$B = \begin{pmatrix} c_2 & 0 & 0 & 0 \\ 0 & c_2 & 0 & 0 \\ 0 & 0 & c_3 & 0 \\ 0 & 0 & 0 & c_3 \\ -c_4 & 0 & 0 & 0 \\ 0 & -c_4 & 0 & 0 \end{pmatrix} \tag{5}$$

$$C = \begin{pmatrix} 1 & 0 & 0 & 0 & 0 & 0 \\ 0 & 1 & 0 & 0 & 0 & 0 \\ 0 & 0 & 1 & 0 & 0 & 0 \\ 0 & 0 & 0 & 1 & 0 & 0 \end{pmatrix} \tag{6}$$

The coefficients used are: $c_1 = L_s L_r - M^2$, $c_2 = L_r/c_1$, $c_3 = 1/L_{ls}$, $c_4 = M/c_1$, $c_5 = L_s c_1$, $a_{s2} = R_s c_2$, $a_{s3} = R_s c_3$, $a_{s4} = R_s c_4$, $a_{r4} = R_r c_4$, $a_{r5} = R_r c_5$, $a_{l4} = L_r c_4 \omega_r$, $a_{l5} = L_r c_5 \omega_r$, $a_{m4} = M c_4 \omega_r$ and $a_{m5} = M c_5 \omega_r$.

The inverter uses the optimal configuration $u_{opt}(k+1)$ specified by the FSMPC for the next sampling period. The VSI configuration is utilized to compute the resulting stator voltages in $\alpha-\beta$ and $x-y$ planes $v = (v_{s\alpha},\ v_{s\beta},\ v_{sx},\ v_{sy})$ $v = V_{DC} u T M$, where V_{DC} is the DC-link voltage, u is a row vector containing the gating signals, T is the connectivity matrix that takes into account how the VSI gating signals are distributed, and M is a coordinate transformation matrix accounting for the spatial distribution of the machine windings. For the five-phase IM used in this paper, the connectivity and transformation matrices are given by:

$$T = \frac{1}{5}\begin{pmatrix} 4 & -1 & -1 & -1 & -1 \\ -1 & 4 & -1 & -1 & -1 \\ -1 & -1 & 4 & -1 & -1 \\ -1 & -1 & -1 & 4 & -1 \\ -1 & -1 & -1 & -1 & 4 \end{pmatrix} \tag{7}$$

$$M = \frac{2}{5}\begin{pmatrix} 1 & \cos\vartheta & \cos 2\vartheta & \cos 3\vartheta & \cos 4\vartheta \\ 0 & \sin\vartheta & \sin 2\vartheta & \sin 3\vartheta & \sin 4\vartheta \\ 1 & \cos 2\vartheta & \cos 4\vartheta & \cos\vartheta & \cos 3\vartheta \\ 0 & \sin 2\vartheta & \sin 4\vartheta & \sin\vartheta & \sin 3\vartheta \\ 1/2 & 1/2 & 1/2 & 1/2 & 1/2 \end{pmatrix} \tag{8}$$

where ϑ is $2\pi/5$. Equations (2-3) are discretized with a forward Euler method to be used for the predictive controller. A second step ahead prediction is needed to account for the fact that the computation time takes most of the sampling

time. By combining the previous definitions, the following expression can be found

$$\hat{i}(k+2|k) = Ai(k) + B_1 u(k) + B_2 u(k+1) + \hat{G}(k|k) \quad (9)$$

where $\hat{i}(k+2|k)$ is the prediction for stator currents made at time k for two samples ahead, $u(k)$ and $u(k+1)$ are the actual and next control action, and $\hat{G}(k|k)$ is a term accounting for the dynamics of the rotor currents that are not usually measured for practical and economical reasons.

The selection of $u(k+1)$ at discrete time k is made minimizing CF for time $k+2$. In this way, the one-sample time delay introduced by the computations is considered, as must be done in FSMPC schemes [27]. Note that $J(k+2)$ is a function of the state, the reference values for $k+2$ and the control action for $k+1$. This cost function can incorporate a number of different terms [28]. However, the simplest CF penalizes the predicted control error $\hat{e}(k+2) = \Big(i^*(k+2) - \hat{i}(k+2)\Big)$, where $i^*(k+2)$ represents the reference for state space vector i, and $\hat{i}(k+2)$ the 2-step ahead prediction. More complex cost functions are used to regulate $x-y$ currents and to prevent the VSI switching frequency to become too high. The first issue is considered by introducing a weighting factor λ_{xy} that allows to put more emphasis on $\alpha-\beta$ tracking over $x-y$ regulation or vice versa. The second issue is more convoluted to consider, but it can be handled by penalizing the VSI commutations. This idea, first introduced in [27], is incorporated into the cost function by computing the number of switch changes $\Delta U(k)$ produced at the VSI when configuration $u(k)$ is changed to $u(k+1)$. The number of switch changes for a five-phase VSI can be computed as

$$\Delta U(k) = \sum_{i=1}^{5} |u_i(k+1) - u_i(k)| \quad (10)$$

where u_i is the i-th component of vector u. In FSMPC, vector u indicates, with zeros and ones, the state of each switch of the VSI (see [27] for further details). Hence, the difference $|u_i(k+1) - u_i(k)|$ takes the value 1 if a change has taken place at the i-th leg and zero otherwise (notice the use of absolute value). With these considerations, the cost function that will be applied can be written as

$$\begin{aligned} J(k+2) &= \|\hat{e}_{\alpha\beta}(k+2)\|^2 + \\ &\quad \lambda_{xy}\|\hat{e}_{xy}(k+2)\|^2 + \lambda_{sc}\Delta U(k+2) \quad (11) \end{aligned}$$

where $\|.\|$ denotes vector modulus, $\hat{e}_{\alpha\beta}(k+2) = i^*_{s\alpha\beta}(k+2) - \hat{i}_{s\alpha\beta}(k+2)$ is the predicted tracking error in $\alpha-\beta$ plane, $\hat{e}_{xy}(k+2) = \hat{i}_{sxy}(k+2)$ is the predicted tracking error in $x-y$ plane.

A. Tuning and Figures of Merit

The usual practice in MPC for drives is to tune the controller by means of selecting a CF with some structure and parameters. The parameters are usually referred to as Weighting Factors or WF for short. The role of WF is to provide more relevance to some terms in the CF. The tuning goal is to achieve the particular compromise solution that is deemed best on a global basis [29].

It has been shown in different reports that FSMPC faces a trade-off between conflicting criteria [30]–[32]. This fact arises from the use of a CF that includes several objectives, and its instantaneous (discrete-time wise) minimization imprints in the system a certain global behavior that constitutes a compromise solution between figures of merit. For instance, the current tracking error, $x-y$ content, and commutation frequency are related.

Tuning has been reported as difficult and time-consuming, which makes that some researchers have turned their attention to schemes avoiding WF [33]. The authors feel that the weighting factors bring flexibility that can not be achieved otherwise. Then, WF are not eliminated in this work, but they rather are kept and selected considering multiple operating points, allowing a more effective tuning procedure.

Regarding the performance indices, in the case of FSMPC, the stator current tracking (in $\alpha-\beta$ and $x-y$ planes) and the switching rate of the VSI are usually considered. The THD of phase currents and the ripple factor γ of $x-y$ currents provide additional information of interest. These quantities can then be defined for each operating point by averaging over a time window $(k_1,\ k_2)$ according to

$$E_{\alpha-\beta} = \sqrt{\frac{1}{(k_2-k_1+1)}\sum_{k=k_1}^{k_2} e^2_{\alpha\beta}(k)} \quad (12)$$

$$E_{x-y} = \sqrt{\frac{1}{(k_2-k_1+1)}\sum_{k=k_1}^{k_2} e^2_{xy}(k)} \quad (13)$$

$$F_{sw} = \frac{1/5}{T_s(k_2-k_1+1)}\sum_{k=k_1}^{k_2} \Delta U(k) \quad (14)$$

$$THD = \frac{100}{I_1}\sqrt{\sum_{i=2}^{\infty} I_i^2} \quad (15)$$

$$\gamma = \frac{100}{I_1} E_{x-y} \quad (16)$$

where the temporal indices k_1, k_2 define a time window where the averaging is done. In the present case, five electrical cycles have been used, so $k_2 = k_1 + 5/f_e/T_s$ with f_e being the electrical frequency. In the previous expressions, the amplitude of the phase current at the fundamental frequency is I_1 and for harmonic number i it is denoted as I_i.

Some objectives and limitations are also considered in the tuning procedure. It will be assumed that the VSI imposes a limit on F_{sw}. Then, the WF tuning should provide F_{sw} below the limit for all possible operating points. This condition can be expressed as $F_{sw} < U_{sw}$. Moreover, $x-y$ currents are a source of inefficiency as they do not produce torque, just copper losses, and thus they should be minimized. Finally, the tuning should have as an objective achieving a small tracking error in $\alpha-\beta$ for each operating point. The above considerations naturally lead to seeking an optimal tuning for each operating point. This would produce a drive behavior

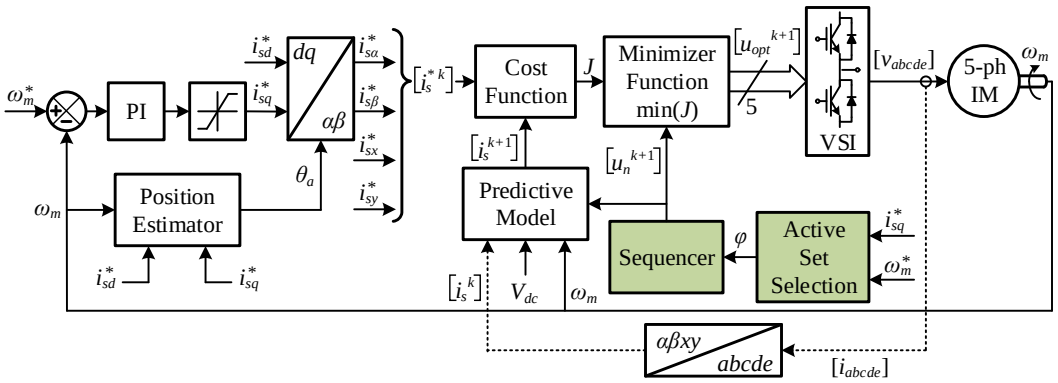

Fig. 1. Diagram of the proposed MPC with Hybrid Control Set.

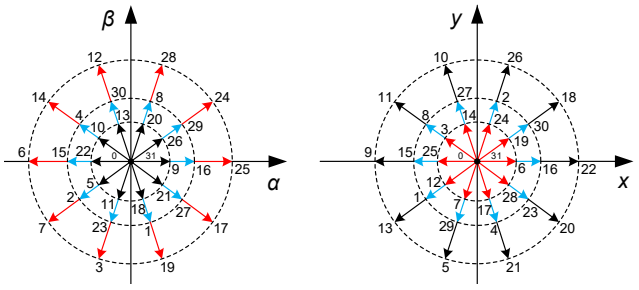

Fig. 2. Distribution of voltage vectors for a 5-phase VSI in $\alpha-\beta$ plane (left) and $x-y$ plane (right).

characterized by $F_{sw} < U_{sw}$, $E_{\alpha-\beta} < U_{\alpha-\beta}$ and the minimum possible value for $E_{x-y} < U_{xy}$. This can be expressed as

$$E^o_{\alpha-\beta} = \min_{(\lambda_{xy},\lambda_{sc})} E_{x-y} \tag{17}$$

Note that this approach is similar to the one used in [26] and involves solving the optimization problem of (17). This can be done off-line and any general optimization algorithm can be used. Moreover, the problem has just two decision variables $(\lambda_{xy}, \lambda_{sc})$, hence any desktop computer can solve it in a matter of minutes.

III. Hybrid Control Set MPC

Fig. 1 shows a diagram of the proposal where the outer control loop is responsible for speed tracking. The inner loop is responsible for current tracking by selecting the VSI state for the (k+1) period. The predictive controller in this inner loop uses a set of VV (marked as φ) that is selected by the block marked Active Set Selection. This block receives the signals i^*_{sq} and ω^*_m from the outer loop, allowing the selection of the most adequate set of AVV for the actual situation. The operation of the Active Set Selection block is described below.

The considered sets are the following:

- 1. FS-32VV. It is the full set of 32 VV that the five-phase VSI can produce. These are shown in Fig. 2 numbered from 0 to 31.
- 2. RS-10LPZ. It is a reduced set consisting of 10 large VV (outermost circle) in the $\alpha-\beta$ plane plus two zero voltage configurations. These VV appear in red colour in Fig. 2 marked as $\{3, 6, 7, 12, 14, 17, 19, 24, 25, 28\}$. Note that this set generates the shortest VV in the $x-y$ plane. The number of AVV is also reduced, and equally the computing time needed by the controller, which improves the tracking and reduces the harmonic content of stator currents. However, this improvement is usually obtained with higher F_{sw} values unless the λ_{sc} values of the CF are modified.
- 3. RS-10MPZ. It is a reduced set consisting of 10 medium VV in the $\alpha-\beta$ plane plus two zero voltage configurations. These VV appear in blue colour in Fig. 2 marked as $\{1, 2, 4, 8, 15, 16, 23, 27, 29, 30\}$. The number of AVV is equal to the previous case, and the same discussion applies. Note that the considered VV are different, as their values in $\alpha-\beta$ and $x-y$ planes. In particular, the lower magnitude in $\alpha-\beta$ plane makes them well suited for low/medium loads. However, the $x-y$ content is higher compared to the VV of the RS-10LPZ set. This means that the λ_{xy} values of the CF must be carefully selected. Take into account that this means modifying also the λ_{sc} as they are relative to each other.

Please note that, although the FS-32VV contains all VV, its performance is not superior to the other sets for all operating points. It will be shown that for some operating points it is best to use a reduced set for speeding up the computation with improved results. To this end, a partition of the operating space is made in the following.

A. Partition of Operating Space

The Active Set Selection block relies on a division of the operating space in a way similar to the Local Controller Network cited in the introduction. The selection of regions where local controllers are defined is not a trivial task in a general case. For the particular case of FSMPC of an IM drive, the mechanical speed ω_m and the stator current related to the electro-mechanical torque i_q can serve as scheduling variables for the determination of the active set. Considering the range of variation of these variables for a particular IM, the operating space can be defined as $\Phi = [0,\ \overline{\omega}] \times [0,\ \overline{i_q}]$ where the over line indicates the maximum value.

The maximum values are determined in this case by the operating capabilities of the experimental system, thus $\overline{i_q}$ is taken as the rated current, so $\overline{i_q} = 2.5$ (A). Similarly $\overline{\omega}$ is limited by the DC link and maximum available load torque, producing $\overline{\omega} = 600$ (rpm).

The operating space is then partitioned into $N_\omega \times N_{iq}$ cells, where N_ω is the number of divisions in the ω_m axis and N_{iq} is the number of divisions in the i_q axis. In the present simulations and experiments, a total of 6×9 cells are used for illustrative purposes, although other values could be used.

B. Active Set Determination

The proposed scheme (HCSMPC) relies on the use of a different AVV set for each operating point. It will be shown later that, for the figures of merit and objectives described in Section II, and considering the best tuning provided by (17), some AVV provide better results than others. However, this selection must be made on the basis of the actual operating point according to the idea of Local Controller Networks [25]. All of this means that the operating point must be identified during operation.

In the present case, thanks to the appropriate discretization of the operating space (used in [26] and presented in Section III-A), the outer loop is capable of identifying the operating point, since the two scheduling variables (ω_m and i_q) must be considered in this loop. Please recall that the outer controller is responsible for measuring the speed and selecting the most appropriate i_{sq} current.

It is worth mentioning that the operating point does not change as fast as the dynamics of the inner (current tracking) loop. This is due to the fact that mechanical variables have much slower dynamics than electrical ones. Hence, the operating point can be found by means of a linear computation as

$$n_i = \lfloor N_\omega \frac{\omega_m}{\overline{\omega}} \rfloor \quad (18)$$

$$n_j = \lfloor N_{iq} \frac{i_{sq}}{\overline{i_q}} \rfloor \quad (19)$$

where $\lfloor . \rfloor$ is the floor function, and n_i, n_j are indices that indicate the actual cell in the operating space partition. These indices are used in the look-up table presented in Table I. The operations to find the indices are just a couple of multiplications and rounding with floor, easily realizable in a digital signal processor. It is interesting to highlight that these computations are negligible compared with the rest of operations that the outer loop must perform: measurements, PI control. As a result the computational burden of the proposed scheme is almost the same and affordable by the outer loop.

IV. Simulation and Experimental Results

The proposed method is now tested and compared. The FSMPC variations will be denominated attending to the active set. The FSMPC using the set FS-32VV (introduced in Section III) will be used as a baseline. For clarity, this controller will be referred to as standard FSMPC or Std-MPC for short. The proposal uses a hybrid control set taken from previous Table I. For clarity, this controller will be referred to as hybrid FSMPC or HCS-MPC for short.

TABLE I
Active Set for each Operating Region (1=FS-32VV, 2=RS-10LPZ, 3=RS-10MPZ)

ω_m	i_{sq} (pu)								
(pu)	0.1	0.2	0.3	0.4	0.5	0.6	0.7	0.8	0.9
0.3	2	2	2	2	1	1	3	2	2
0.5	2	2	2	3	1	1	2	2	2
0.6	2	2	3	3	2	2	2	2	2
0.8	2	2	3	3	2	2	2	2	2
1.0	2	2	3	2	2	2	2	1	1
1.1	2	3	3	2	2	2	1	1	1

A. Simulations

The simulations have been performed in a MATLAB environment writing the differential equations for the evolution of the IM and load. The controller is incorporated as a discrete-time subsystem, and the computing time needed by the controller is accurately taken into account. The sampling time for the controller is also incorporated into the simulation. The values are in accordance with those used in the real experiments. A Runge-Kutta type of numerical integration has been used, taking into account the fact that slow and fast dynamics are involved in the system being simulated. The IM parameters are those of the real IM in the experimental setup that will be used later for confirmation.

The tuning of the controllers is also considered for the simulations. Using equation (17), an optimal value is found for $\Lambda = (\lambda_{xy}, \lambda_{sc})^\intercal$ for each operating point. In this case, $U_{sw} = 8$ (kHz), $U_{\alpha-\beta} = 0.013$ (A) are used. These values are selected for illustrative purposes; the proposed method can accommodate other values as well. The tuning procedure is carried out for each of the three considered active control sets. Fig. 3 shows the $x-y$ current content as measured by E_{x-y} for several operating points.

It can be seen that the RS-10LPZ configuration yields, on average, the best results according to E_{x-y}. Keep in mind that, given the tuning procedure, all active sets provide $F_{sw} < 8$ (kHz) and $E_{\alpha-\beta} < 0.013$ (A). It is interesting to note that none of the active sets is better for all operating points. For every operating point, there is one active set that gives the best results. Table I presents the best active set for each operating point. Each entry of the table represents a cell of the operating space partition, and the active set (FS-32VV, RS-10LPZ and RS-10MPZ) has been identified by a number from 1 to 3.

Using this procedure for the selection of the active VV set, it is possible to obtain the performance figures for the HCSMPC by simulation. At each sampling time, the FSMPC receives the set φ from the Active Set Selection block. Figure 4 shows the performance map for E_{x-y} for the proposed method, where the harmonic content is greatly reduced (please notice the change in the scale in the z-axis). This performance map includes all operating points identified by the mechanical speed and the torque producing current i_{sq}, hence the assessment is global.

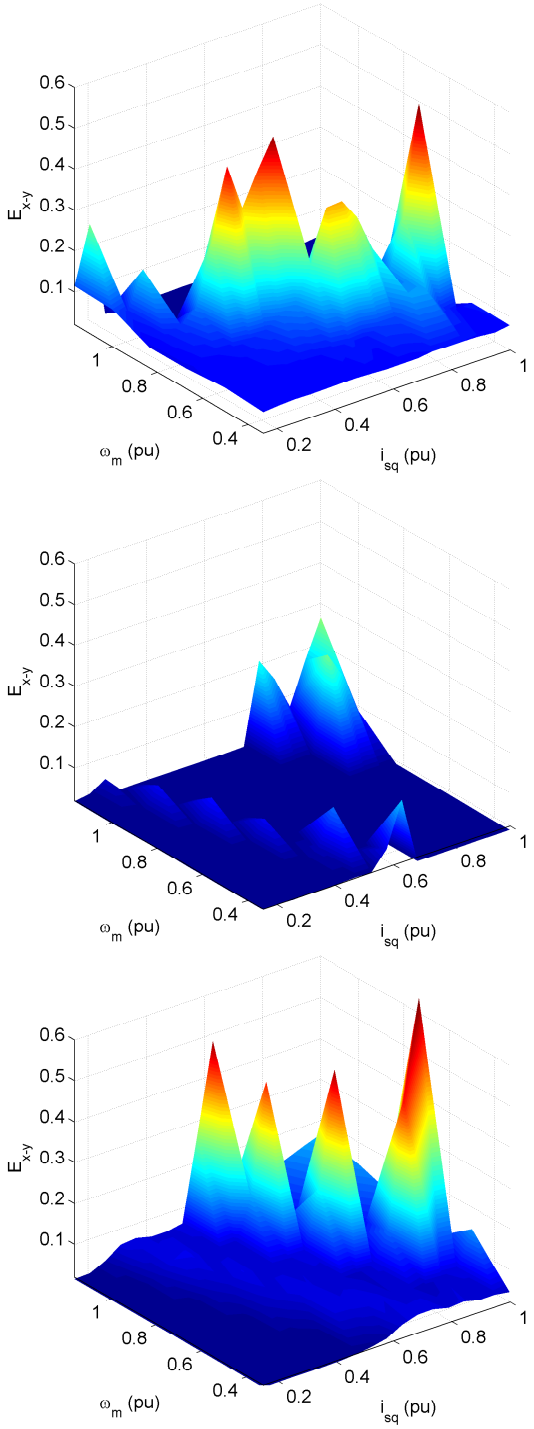

Fig. 3. Simulation values for E_{x-y} for the FS-32VV (top), RS-10LPZ (middle) and 10M-RSMPC (bottom).

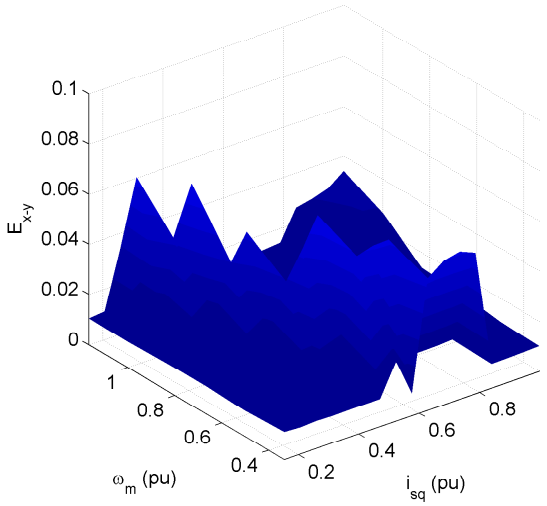

Fig. 4. Simulation values for E_{x-y} for the proposed HCSMPC.

TABLE II
SUMMARY OF SIMULATION RESULTS

AVV set	$E_{\alpha-\beta}$ (A) min	$E_{\alpha-\beta}$ (A) max	E_{x-y} (A) min	E_{x-y} (A) max	F_{sw} (kHz) min	F_{sw} (kHz) max
FS-32VV	0.0125	0.4906	0.0199	0.5303	2.32	7.80
RS-10LPZ	0.0125	0.0468	0.0091	0.2645	2.52	7.98
RS-10MPZ	0.0098	1.2004	0.0145	0.6723	3.26	8.00
HCS-MPC	0.0111	0.4906	**0.0088**	**0.0650**	2.57	8.00

Table II shows the simulation results for all figures of merit (12), (13) and (14) for all operating points. It can be seen that the proposed Hybrid Control Set controller produces the lowest $x - y$ content, while maintaining the desired performance in terms of F_{sw} and $E_{\alpha-\beta}$.

B. Experimental Results

Different experimental tests are performed on a five-phase, 30 slots, and three pairs of pole induction motor. The electrical and mechanical parameters of the five-phase motor are given in Table III.

The multi-phase power converter is based on two conventional three-phase VSIs from SEMIKRON (two SKS-22F modules in which five power legs are used). The DC link voltage is set to 300 V using an external DC power supply. The electronic control unit is based on a MSK28335 board and a Texas Instruments TMS320F28335 digital signal processor. A digital encoder (GHM510296R/2500) and the enhanced quadrature encoder pulse peripheral of the DSP are used to measure the rotor mechanical speed ω_m. The load torque (T_L), which is demanded in the tests, is set by an independently controlled DC machine that is mechanically coupled to the five-phase machine. The experimental test rig is shown in Fig. 5, where some photographs of the real system are included.

The DSP program is written in C using Code Composer Studio. The sampling period is set for each controller according to their computing needs, assuring that the comparison is fair in this respect. For 32 VV (used by the FS-32VV configuration), a sampling time of 66×10^{-6} (s) can be achieved. For 12 VV (used by the RS-10LPZ and RS-10MPZ), a sampling

TABLE III
ELECTRICAL AND MECHANICAL PARAMETERS OF THE FIVE-PHASE IM

Parameter	Value	Unit
Stator resistance, R_s	12.85	Ω
Rotor resistance, R_r	4.80	Ω
Stator leakage inductance, L_{ls}	79.93	mH
Rotor leakage inductance, L_{lr}	79.93	mH
Mutual inductance, M	681.7	mH
Rotational inertia, J_m	0.02	kg m^2
Number of pairs of poles, P	3	-

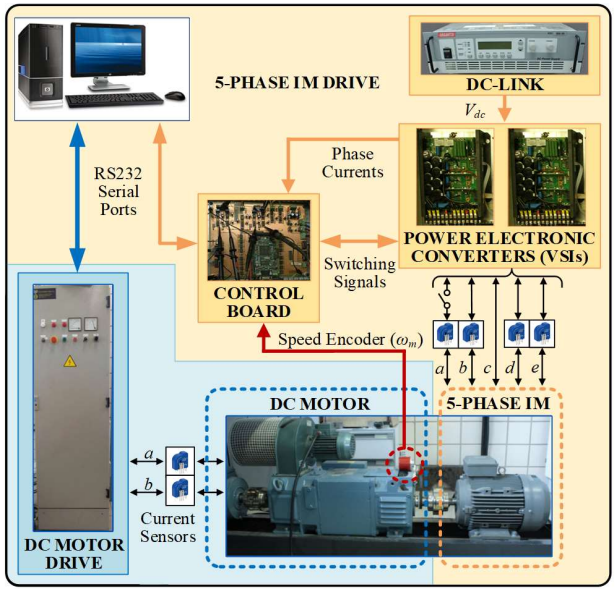

Fig. 5. Experimental test rig.

time of 40×10^{-6} (s) is used. Please notice that, despite the sampling frequencies being 15kHz and 25kHz, respectively, the average switching frequencies are much lower as will be shown later. Note also that the extra computational burden in terms of processing time (for the hardware used in the experiments) is about 80 CPU cycles, which amount to less than 600×10^{-9} (s) according to the DSP specifications and its Floating-Point Unit. The measured extra time is then negligible in our experiments compared with the rest of computing time needed by the FSMPC (66×10^{-6} (s) for the FS-32VV configuration).

Several operating points have been considered for the assessment of the HCSMPC scheme as presented in Table IV. The results of the proposed method and a standard FSMPC technique are shown in Table V. It can be seen a superior behavior of the HCSMPC scheme, verified for $\alpha-\beta$ tracking, for $x-y$ regulation and with less use of VSI commutations. Take, for instance, the case A, which is characterized by a low speed. This operating point, when using FSMPC, typically produces high THD, high switching frequency, and medium values for $x-y$, but since the fundamental component I_1 has a lower value (compared with other operating points), the γ_x factor is also high. In this scenario, the HCSMPC scheme chooses as AVV set 2 (set RS-10LPZ). As a result, all figures of merit are improved compared to the standard FSMPC. The same happens in all analyzed operating points.

TABLE IV
CASES CONSIDERED IN THE EXPERIMENTAL COMPARISON

Case	ω_m^* (rpm)	T_L (%)	i_{sq}^* (A)
A	280	0	0.55
B	280	60	1.49
C	500	0	0.62
D	500	60	1.69

TABLE V
SUMMARY OF RESULTS FOR COMPARISON

Case	Controller	$E_{\alpha-\beta}$ (A)	E_{x-y} (A)	F_{sw} (kHz)	THD (%)	γ_x (%)
A	Std-MPC	0.1481	0.1235	4.57	15.7	16.5
	HCS-MPC	0.1030	0.1007	3.46	12.1	13.5
B	Std-MPC	0.1468	0.1490	4.19	6.58	7.14
	HCS-MPC	0.1142	0.1286	3.29	5.21	6.23
C	Std-MPC	0.1433	0.1417	4.40	16.1	18.3
	HCS-MPC	0.1125	0.1131	3.33	11.5	14.6
D	Std-MPC	0.1372	0.1340	2.89	6.18	6.25
	HCS-MPC	0.1092	0.1329	2.87	4.39	6.25

The THD of stator currents and the ripple factor of i_{sx} are also smaller for the proposed scheme as these figures of merit are strongly linked to the quality of tracking. This is a remarkable result since it has been previously shown that FSMPC cannot, by tuning alone, improve all figures of merit at once. The interested reader is directed to [31] for further details. The improvement seen here is a result of the fact that the HCSMPC provides not just a change in parameters.

In addition to the previous result Tables, Figures 6 and 7 show the trajectories of i_s for α and x axes (similar results are found for β and y axes). It can be seen that the stator currents are regulated using both techniques, standard FSMPC and HCSMPC. In both cases, the variables follow their reference values in α and x axes, respectively. However, the average switching frequency used by the HCSMPC is always lower. For instance, in case A, a value of 3.46 kHz is found for HCSMPC versus 4.57 kHz for standard FSMPC (see F_{sw} value in Table V). Furthermore, the performance indices that quantify tracking are superior for HCSMPC in an unfair match since HCSMPC uses a lower average switching frequency than the standard FSMPC. With all of this, it can be concluded that the proposal outperforms the standard FSMPC technique as a result of the selection of the most appropriate AVV set.

In addition to the previous tests, some transient responses are given in the following. Fig. 8 shows the results for a speed reversal (R) and Fig. 9 for a step in load. In the case of the speed reversal, since the speed before and after the reversal are the same (except for the sign) and since the i_{sq} current takes large values, large voltage vectors are selected (set RS-10LPZ). Other than that, the outer loop PI gets saturated in both cases (HCS and STD) providing the maximum i_{sq}. For the load step, the programmable load torque provided by the auxiliary DC machine (see Fig. 5) is increased while maintaining the speed reference ω_m^*. It can be seen that the increased torque causes a momentary loss of speed that is recovered thanks to an increase of i_{sq}. The change in i_{sq} causes the HCSMPC algorithm to change from set 3 (active before the step) to set 2. It can be seen that the recovery is faster for the proposed

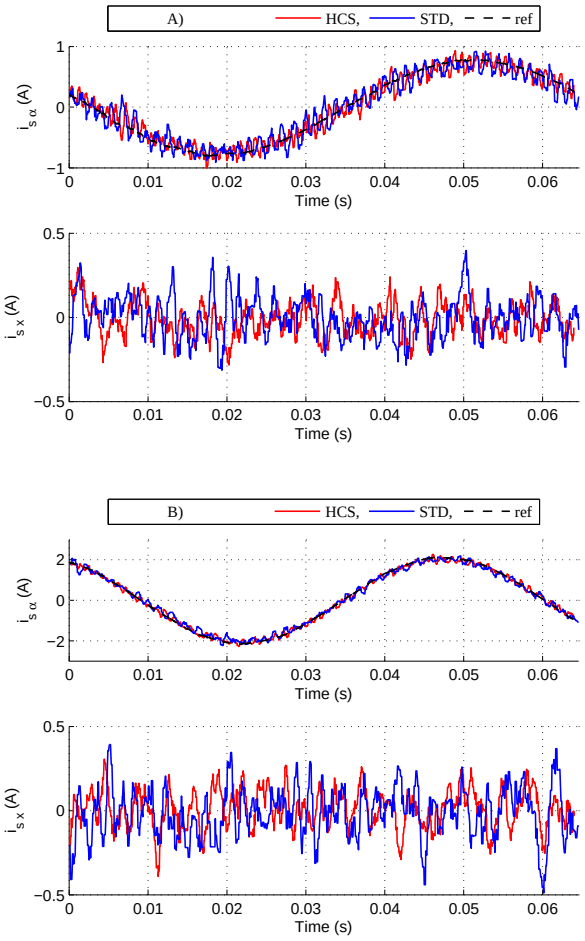

Fig. 6. Experimental results for cases A (top) and B (bottom).

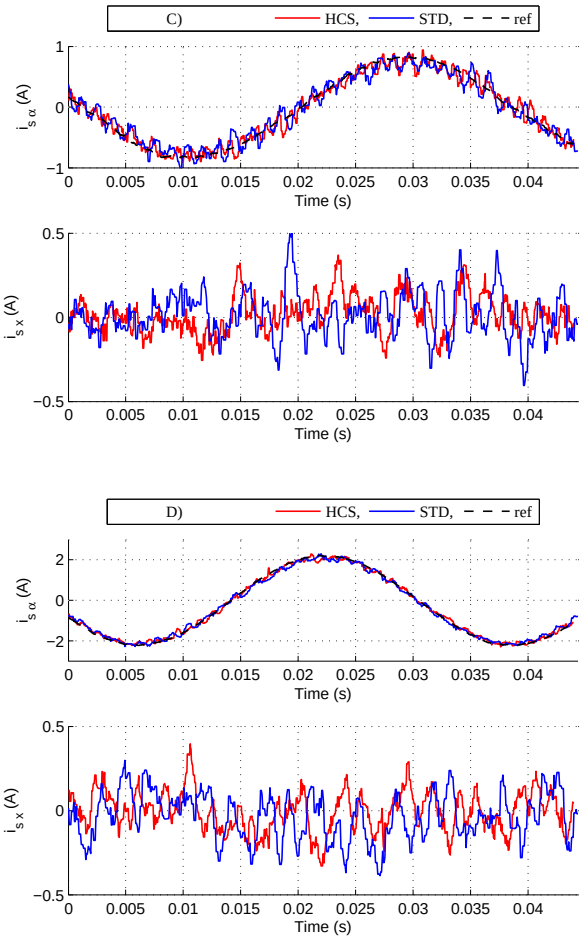

Fig. 7. Experimental results for cases C (top) and D (bottom).

HCSMPC compared to the standard FSMPC. These results are especially remarkable in the light that the proposal was made having in mind steady state. Despite this, as these results testify, the selection of the most appropriate AVV is a degree of freedom that can also be used for transient regimes. For the sake of completeness, the electrical torque and rotor flux are also depicted. Note that the experimental test bed does not include a torque meter and the multiphase induction machine does not incorporate flux sensors. Then, their values have been evaluated using the modeling of the electro-mechanical system, as it is detailed in [34]. Note that the speed dynamic of the system using the proposed HCSMPC and the standard FSMPC are different. Although the final i_{sq}^* is the same using both controllers, the references forced by the controllers are different (they differ in their tuning, see Section II-A, and in the sampling time, see Section IV-B).

V. Conclusions

FSMPC emerges in the earliest 21th century like an alternative in the multi-phase drives' field. Its simple and intuitive formulation has contributed to promote the interest in it, and many researchers have explored its use. Different sets of active voltage vectors, different cost functions, and modulation with the virtual voltage vector concept have been proposed. However, FSMPC faces important limitations in relation to the computational cost and the generated harmonic content. This work analyzes the influence of different sets of active voltage vectors on the performance of multi-phase drives. A novel current control structure has been proposed in which a different active voltage vector set is applied for every speed-load situation. The proposal has been tested in a five-phase IM with distributed windings using simulation and experimental results. The obtained results state the interest in the proposal that improves the performance of standard FSMPC techniques in terms of stator current tracking in $\alpha - \beta$ and $x - y$ planes, while reducing the switching frequency of the power converter. Note that the directing principles guiding the tuning used in this paper are arguably of general acceptance, but they can be easily modified to suit and extend this work to other specific applications.

Acknowledgment

This research has been funded as Proyecto RTI2018-101897-B-I00 by FEDER/Ministerio de Ciencia e Innovación – Agencia Estatal de Investigación, Spain.

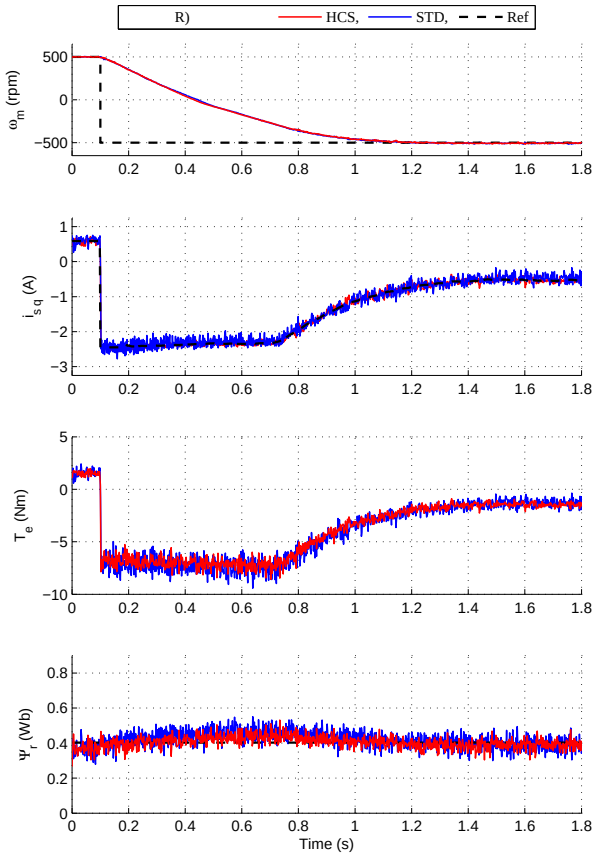

Fig. 8. Experimental results for a reversal test.

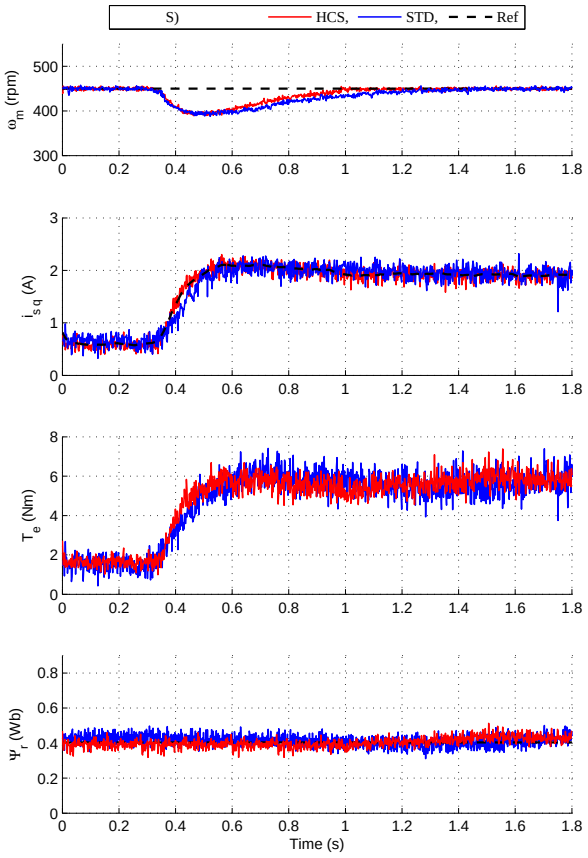

Fig. 9. Experimental results for a load step test.

REFERENCES

[1] M. Schwenzer, M. Ay, T. Bergs, and D. Abel, "Review on model predictive control: an engineering perspective," *Int J Adv Manuf Technol*, vol. 117, pp. 1327–1349, 2021.

[2] P. Karamanakos, E. Liegmann, T. Geyer, and R. Kennel, "Model predictive control of power electronic systems: Methods, results, and challenges," *IEEE Open Journal of Industry Applications*, vol. 1, pp. 95–114, 2020.

[3] J. K. Pandit, M. V. Aware, R. V. Nemade, and E. Levi, "Direct torque control scheme for a six-phase induction motor with reduced torque ripple," *IEEE Transactions on Power Electronics*, vol. 32, no. 9, pp. 7118–7129, 2016.

[4] F. Wang, X. Mei, J. Rodriguez, and R. Kennel, "Model predictive control for electrical drive systems-an overview," *CES Transactions on Electrical Machines and Systems*, vol. 1, no. 3, pp. 219–230, 2017.

[5] C. S. Lim, S. S. Lee, Y. C. C. Wong, I. U. Nutkani, and H. H. Goh, "Comparison of current control strategies based on FCS-MPC and D-PI-PWM control for actively damped VSCs with LCL-filters," *IEEE Access*, vol. 7, pp. 112 410–112 423, 2019.

[6] C.-S. Lim, E. Levi, M. Jones, N. Rahim, and W.-P. Hew, "A comparative study of synchronous current control schemes based on FCS-MPC and PI-PWM for a two-motor three-phase drive," *Industrial Electronics, IEEE Transactions on*, vol. 61, no. 8, pp. 3867–3878, Aug 2014.

[7] S. Li, G. Yang, X. Zhang, J. Zhang, and J. Yangb, "Dual closed-loop control strategy on harmonic plane for multiphase induction motor with harmonic injection based on air-gap flux orientation control," *IEEE Journal of Emerging and Selected Topics in Power Electronics*, 2022.

[8] C. Martin-Torres, F. Barrero, M. R. Arahal, and M. J. Duran, "Model-based predictive current controllers in multiphase drives dealing with natural reduction of harmonic distortion," *Energies*, vol. 12, no. 9, 2019.

[9] C. Xue, W. Song, and X. Feng, "Finite control-set model predictive current control of five-phase permanent-magnet synchronous machine based on virtual voltage vectors," *IET Electric Power Applications*, vol. 11, no. 5, pp. 836–846, 2017.

[10] P. Garcia-Entrambasaguas, I. Zoric, I. Gonzalez-Prieto, M. J. Duran, and E. Levi, "Direct torque and predictive control strategies in nine-phase electric drives using virtual voltage vectors," *IEEE Transactions on Power Electronics*, vol. 34, no. 12, pp. 12 106–12 119, 2019.

[11] C. Romero, L. Delorme, O. Gonzalez, M. Ayala, J. Rodas, and R. Gregor, "Algorithm for implementation of optimal vector combinations in model predictive current control of six-phase induction machines," *Energies*, vol. 14, no. 13, p. 3857, 2021.

[12] M. Yao, J. Peng, and X. Sun, "Model predictive flux control of six-phase permanent magnet synchronous motor with novel virtual voltage vectors," *Electrical Engineering*, pp. 1–13, 2022.

[13] W. Huang, W. Hua, F. Yin, F. Yu, and J. Qi, "Model predictive thrust force control of a linear flux-switching permanent magnet machine with voltage vectors selection and synthesis," *IEEE Transactions on Industrial Electronics*, vol. 66, no. 6, pp. 4956–4967, 2018.

[14] H.-C. Moon, J.-S. Lee, and K.-B. Lee, "A robust deadbeat finite set model predictive current control based on discrete space vector modulation for a grid-connected voltage source inverter," *IEEE Transcactions on Energy Conversion*, vol. 33, no. 4, pp. 1719–1728, 2018.

[15] X. Sun, T. Li, M. Yao, G. Lei, Y. Guo, and J. Zhu, "Improved finite-control-set model predictive control with virtual vectors for PMSHM drives," *IEEE Transcactions on Energy Conversion*, vol. Early Access, 2022.

[16] I. Gonzalez-Prieto, M. J. Duran, J. J. Aciego, C. Martin, and F. Barrero, "Model predictive control of six-phase induction motor drives using virtual voltage vectors," *IEEE Transactions on Industrial Electronics*, vol. 65, no. 1, pp. 27–37, 2017.

[17] J. J. Aciego, I. G. Prieto, and M. J. Duran, "Model predictive control of six-phase induction motor drives using two virtual voltage vectors," *IEEE Journal of Emerging and Selected Topics in Power Electronics*, vol. 7, no. 1, pp. 321–330, 2018.

[18] W. Wang, Y. Fan, S. Chen, and Q. Zhang, "Finite control set model predictive current control of a five-phase PMSM with virtual voltage vectors and adaptive control set," *CES Transactions on Electrical Machines and Systems*, vol. 2, no. 1, pp. 136–141, 2018.

[19] C. D. Townsend, G. Mirzaeva, and G. C. Goodwin, "Short-horizon model predictive modulation of three-phase voltage source inverters," *IEEE Transactions on Industrial Electronics*, vol. 65, no. 4, pp. 2945–2955, 2017.
[20] E. Liegmann, P. Karamanakos, and R. Kennel, "Real-time implementation of long-horizon direct model predictive control on an embedded system," *IEEE Open Journal of Industry Applications*, 2021.
[21] X. Wu, W. Huang, Y. Zhao, and C. Huang, "An efficient model predictive torque control for induction motors with flexible duty ratio optimization," *IEEE Journal of Emerging and Selected Topics in Power Electronics*, 2021.
[22] C. S. Lim, E. Levi, M. Jones, N. A. Rahim, and W. P. Hew, "FCS-MPC-based current control of a five-phase induction motor and its comparison with PI-PWM control," *IEEE Transactions on Industrial Electronics*, vol. 61, no. 1, pp. 149–163, 2014.
[23] Z. Li, Y. Guo, J. Xia, H. Li, and X. Zhang, "Variable sampling frequency model predictive torque control for VSI-fed IM drives without current sensors," *IEEE Journal of Emerging and Selected Topics in Power Electronics*, vol. 9, no. 2, pp. 1507–1517, 2020.
[24] A. J. Gallego, L. J. Yebra, and E. F. Camacho, "Gain scheduling model predictive control of the new TCP-100 parabolic trough field," *IFAC-PapersOnLine*, vol. 51, no. 2, pp. 475–480, 2018.
[25] K. J. Hunt and T. A. Johansen, "Design and analysis of gain-scheduled control using local controller networks," *International Journal of Control*, vol. 66, no. 5, pp. 619–652, 1997.
[26] A. Kowal, M. R. Arahal, C. Martín, and F. Barrero, "Constraint satisfaction in current control of a five-phase drive with locally tuned predictive controllers," *Energies*, vol. 12, no. 14, 2019.
[27] M. R. Arahal, F. Barrero, S. Toral, M. J. Durán, and R. Gregor, "Multi-phase current control using finite-state model-predictive control," *Control Engineering Practice*, vol. 17, no. 5, pp. 579 – 587, 2009.
[28] E. F. Camacho and C. Bordons, *Model predictive control*. Springer, 2013.
[29] A. Shawier, A. Habib, M. Mamdouh, A. S. Abdel-Khalik, and K. H. Ahmed, "Assessment of predictive current control of six-phase induction motor with different winding configurations," *IEEE Access*, 2021.
[30] M. F. Elmorshedy, W. Xu, F. F. El-Sousy, M. R. Islam, and A. A. Ahmed, "Recent achievements in model predictive control techniques for industrial motor: A comprehensive state-of-the-art," *IEEE Access*, vol. 9, pp. 58 170–58 191, 2021.
[31] M. R. Arahal, F. Barrero, M. J. Durán, M. G. Ortega, and C. Martín, "Trade-offs analysis in predictive current control of multi-phase induction machines," *Control Engineering Practice*, vol. 81, pp. 105–113, 2018.
[32] C. Liu and Y. Luo, "Overview of advanced control strategies for electric machines," *Chinese Journal of Electrical Engineering*, vol. 3, no. 2, pp. 53–61, 2017.
[33] M. Mamdouh and M. A. Abido, "Weighting factor elimination for predictive current control of asymmetric six phase induction motor," in *2020 IEEE EEEIC I&CPS Europe*. IEEE, 2020, pp. 1–6.
[34] M. Bermúdez, F. Barrero, C. Martín, and M. Perales, "Performance analysis of direct torque controllers in five-phase electrical drives," *Applied Sciences*, vol. 11, no. 24, 2021.